REPORT DOCUMENTATION PAGE		Form Approved OMB NO. 0704-0188

The public reporting burden for this collection of information is estimated to average 1 hour per response, including the time for reviewing instructions, searching existing data sources, gathering and maintaining the data needed, and completing and reviewing the collection of information. Send comments regarding this burden estimate or any other aspect of this collection of information, including suggesstions for reducing this burden, to Washington Headquarters Services, Directorate for Information Operations and Reports, 1215 Jefferson Davis Highway, Suite 1204, Arlington VA, 22202-4302. Respondents should be aware that notwithstanding any other provision of law, no person shall be subject to any oenalty for failing to comply with a collection of information if it does not display a currently valid OMB control number.
PLEASE DO NOT RETURN YOUR FORM TO THE ABOVE ADDRESS.

1. REPORT DATE (DD-MM-YYYY) 30-11-2013	2. REPORT TYPE Final Report	3. DATES COVERED (From - To) 1-Sep-2010 - 31-Aug-2013

4. TITLE AND SUBTITLE Shock Response of Dry and Water-Saturated Soils	5a. CONTRACT NUMBER W911NF-10-1-0377
	5b. GRANT NUMBER
	5c. PROGRAM ELEMENT NUMBER 622618
6. AUTHORS Sarah T. Stewart, Matthew G. Newman, Richard G. Kraus	5d. PROJECT NUMBER
	5e. TASK NUMBER
	5f. WORK UNIT NUMBER

7. PERFORMING ORGANIZATION NAMES AND ADDRESSES Harvard University 1350 Massachusetts Avenue Suite 600 Cambridge, MA 02138 -3846	8. PERFORMING ORGANIZATION REPORT NUMBER

9. SPONSORING/MONITORING AGENCY NAME(S) AND ADDRESS (ES) U.S. Army Research Office P.O. Box 12211 Research Triangle Park, NC 27709-2211	10. SPONSOR/MONITOR'S ACRONYM(S) ARO
	11. SPONSOR/MONITOR'S REPORT NUMBER(S) 56427-EG.2

12. DISTRIBUTION AVAILIBILITY STATEMENT

Approved for Public Release; Distribution Unlimited

13. SUPPLEMENTARY NOTES

The views, opinions and/or findings contained in this report are those of the author(s) and should not contrued as an official Department of the Army position, policy or decision, unless so designated by other documentation.

14. ABSTRACT

We conducted planar shock wave experiments to measure the dynamic loading of dry and water-saturated soils provided by the Army Research Laboratory (VIMF, ATC Sand-Clay, ATC DSTS). The complicated response of geologic materials to dynamic compression is of fundamental importance to understanding the energy transmitted to the surface by buried explosives. We measured the shock states induced via planar impact experiments on the Harvard 40-mm gas gun. Shock wave velocities in the soil samples were measured using both VISAR and piezoelectric pins. The soils were composed primarily of quartz with different mass fractions of phyllosilicates and

15. SUBJECT TERMS

shock Hugoniot, dry, wet, soils, VIMF, ATC Sand-Clay, ATC DSTS

16. SECURITY CLASSIFICATION OF:			17. LIMITATION OF ABSTRACT	15. NUMBER OF PAGES	19a. NAME OF RESPONSIBLE PERSON Sarah Stewart
a. REPORT UU	b. ABSTRACT UU	c. THIS PAGE UU	UU		19b. TELEPHONE NUMBER 617-496-6462

Report Title

Shock Response of Dry and Water-Saturated Soils

ABSTRACT

We conducted planar shock wave experiments to measure the dynamic loading of dry and water-saturated soils provided by the Army Research Laboratory (VIMF, ATC Sand-Clay, ATC DSTS). The complicated response of geologic materials to dynamic compression is of fundamental importance to understanding the energy transmitted to the surface by buried explosives. We measured the shock states induced via planar impact experiments on the Harvard 40-mm gas gun. Shock wave velocities in the soil samples were measured using both VISAR and piezoelectric pins. The soils were composed primarily of quartz with different mass fractions of phyllosilicates and amorphous material. Using initial particle sizes ranging from 150 to 300 microns, the samples were pressed to densities ranging from 1.7 to 1.93 g/cm3 (about 25-30% porous). Water-saturated samples had densities ranging from 2.23 to 2.33 g/cm3. We find that the dry soils have a linear shock velocity-particle velocity relation that is similar to dry quartz sand with the same initial density. The water-saturated samples are less compressible and have much greater scatter in shock velocities. The VISAR measurement records the dispersion around the mean shock state that arises from reflections between grains, and we will compare the VISAR data to meso-scale hydrocode simulations of the experiment. These data will be used to generate more accurate rheological models for hydrocode simulations of the shock response of heterogeneous granular materials in the low-pressure regime (<10 GPa).

Enter List of papers submitted or published that acknowledge ARO support from the start of the project to the date of this printing. List the papers, including journal references, in the following categories:

(a) Papers published in peer-reviewed journals (N/A for none)

Received   Paper

TOTAL:

Number of Papers published in peer-reviewed journals:

(b) Papers published in non-peer-reviewed journals (N/A for none)

Received   Paper

TOTAL:

Number of Papers published in non peer-reviewed journals:

(c) Presentations

Non Peer-Reviewed Conference Proceeding publications (other than abstracts):

<u>Received</u>   <u>Paper</u>

11/30/2013   1.00   Richard G. Kraus, Matthew G. Newman, Sarah T. Stewart. HUGONIOT MEASUREMENTS ON
                              HETEROGENEOUS GEOLOGIC MATERIALS,
                              Lunar and Planetary Science Conference. 19-MAR-12, . : ,

          TOTAL: **1**

Number of Non Peer-Reviewed Conference Proceeding publications (other than abstracts):

Peer-Reviewed Conference Proceeding publications (other than abstracts):

<u>Received</u>   <u>Paper</u>

          TOTAL:

Number of Peer-Reviewed Conference Proceeding publications (other than abstracts):

(d) Manuscripts

<u>Received</u>   <u>Paper</u>

          TOTAL:

Number of Manuscripts:

Books

<u>Received</u>   <u>Paper</u>

TOTAL:

Patents Submitted

Patents Awarded

Awards

Graduate Students

NAME	PERCENT_SUPPORTED	Discipline
Richard G. Kraus	0.10	
FTE Equivalent:	**0.10**	
Total Number:	**1**	

Names of Post Doctorates

NAME	PERCENT_SUPPORTED
FTE Equivalent:	
Total Number:	

Names of Faculty Supported

NAME	PERCENT_SUPPORTED	National Academy Member
Sarah T. Stewart	0.04	No
FTE Equivalent:	**0.04**	
Total Number:	**1**	

Names of Under Graduate students supported

NAME	PERCENT_SUPPORTED	Discipline
Matthew G. Newman	0.25	Mechanical Engineering
FTE Equivalent:	**0.25**	
Total Number:	**1**	

Student Metrics

This section only applies to graduating undergraduates supported by this agreement in this reporting period

The number of undergraduates funded by this agreement who graduated during this period: 1.00

The number of undergraduates funded by this agreement who graduated during this period with a degree in science, mathematics, engineering, or technology fields: 1.00

The number of undergraduates funded by your agreement who graduated during this period and will continue to pursue a graduate or Ph.D. degree in science, mathematics, engineering, or technology fields: 1.00

Number of graduating undergraduates who achieved a 3.5 GPA to 4.0 (4.0 max scale): 0.00

Number of graduating undergraduates funded by a DoD funded Center of Excellence grant for Education, Research and Engineering: 0.00

The number of undergraduates funded by your agreement who graduated during this period and intend to work for the Department of Defense 1.00

The number of undergraduates funded by your agreement who graduated during this period and will receive scholarships or fellowships for further studies in science, mathematics, engineering or technology fields: 0.00

Names of Personnel receiving masters degrees

NAME

Total Number:

Names of personnel receiving PHDs

NAME
Richard G. Kraus
Total Number: 1

Names of other research staff

NAME	PERCENT_SUPPORTED
Markos Hankin	0.25
Lee Wizda	0.25
FTE Equivalent:	**0.50**
Total Number:	**2**

Sub Contractors (DD882)

Inventions (DD882)

Scientific Progress

See attachment.

Technology Transfer

Shock Response of Dry and Water-Saturated Soils
Final Report

Sarah T. Stewart, Principal Investigator, Harvard University

Matthew G. Newman, Richard G. Kraus, Harvard University

Abstract.   We conducted planar shock wave experiments to measure the dynamic loading of dry and water-saturated soils provided by the Army Research Laboratory (VIMF, ATC Sand-Clay, ATC DSTS). The complicated response of geologic materials to dynamic compression is of fundamental importance to understanding the energy transmitted to the surface by buried explosives. We measured the shock states induced via planar impact experiments on the Harvard 40-mm gas gun. Shock wave velocities in the soil samples were measured using both VISAR and piezoelectric pins. The soils were composed primarily of quartz with different mass fractions of phyllosilicates and amorphous material. Using initial particle sizes ranging from 150 to 300 microns, the samples were pressed to densities ranging from 1.7 to 1.93 g cm^{-3} (about 25-30% porous). Water-saturated samples had densities ranging from 2.23 to 2.33 g cm^{-3}. We find that the dry soils have a linear $U_s - u_p$ relation that is similar to dry quartz sand with the same initial density. The water-saturated samples are less compressible and have much greater scatter in shock velocities. The VISAR measurement records the dispersion around the mean shock state that arises from reflections between grains, and we will compare the VISAR data to mesoscale hydrocode simulations of the experiment. These data will be used to generate more accurate rheological models for hydrocode simulations of the shock response of heterogeneous granular materials in the low-pressure regime (< 10 GPa).

1. Introduction

Buried explosives pose a serious threat to both personnel and equipment. The output of such blasts is a function of the depth of burial, initial stress, and soil conditions. However, the influence of the physical properties (e.g., density and water content) and dynamic response of soils on the blast output is not well understood or quantified. The limited amount of data available for soils and other porous/granular geologic materials demonstrate that the dynamic response is strongly dependent on material and water content. Knowledge of the both loading and unloading behavior is necessary to determine terminal velocities of soils after explosive loading. In addition, current numerical techniques are unable to predict a priori the dynamic response of soils under the wide range of conditions encountered in the field. This work falls under the solid mechanics research area in the U.S. Army Research Office by providing basic shock response data on materials identified to be of strategic interest.

2. Experimental Technique

Using standard references soils provided by Army Research Laboratory (VIMF, ATC Sand-Clay, ATC DSTS), we conducted shock loading experiments on compacted dry samples and water-saturated samples.

2.1. Material properties

Our experiments were conducted on material that was sifted to grain sizes ranging from 150 to 300 microns. The natural soils were sifted to enable the shock wave to traverse multiple grains during the dynamic experiment. The grain size is constrained by the duration of uniaxial flow on a 40-mm gun.

Table 1 presents the the mineral abundances for the three soils measured using an X-ray diffraction technique. Table 2 shows the particle density which is measured using helium pycnometry. Information about the particle density as well as the bulk density is used to calculate the porosity of the soil samples.

2.2. Sample preparation

Dry samples were prepared in a 26 mm diameter capsule. To promote good mixing of the soil constituents and flat surfaces the samples are first pressed by hand, then lightly hammered, and finally pressed to 1 ton up to three times. The amplitude of the pre-experiment press mimics precompression of soils under road conditions. The multiple pressing allowed for rotation of grains and a more homogeneous pre-experiment compacted state.

Wet samples were prepared in a 28 mm diameter capsule using the following three-step process:

1. Dry soil was added to the capsule.

2. Water was added to the capsule in excess and allowed to sit for a period of approximately 20 hours.

3. A specifically constructed polycarbonate piston window with semi-cylindrical cuts through the side was used to press the mixture to maximum unshocked density. This setup allowed excess water to escape from the capsule during this compression process.

The water-saturated samples had densities ranging from 2.2-2.6 g cm^{-3}, corresponding to the 25-30% porosity (Table 2).

2.3. Plate-impact details

Plate impact experiments were performed on the 40-mm gas gun facility at Harvard University. Experiments measured the shock properties of three soils (VIMF, ATC Sand-Clay, and ATC DSTS) under both dry and water-saturated conditions. For each soil sample iteration, we conducted impact tests at approximately 300, 500, 800, and 1200 m s^{-1}.

Figure 1 shows the plate configuration which includes the soil sample mounted between an aluminum 2024 driver and a PMMA window. The soil is contained within a poly-carbonate capsule. Shock measurements were made using both piezoelectric pins and a velocity interferometry system for any reflector (VISAR) [Barker and Hollenbach, 1972]. Both the piezoelectric pins and the VISAR are used to detect shock arrival times on the aluminum driver and the soil sample. In some cases, the VISAR is used to measure the particle velocity history at the soil/PMMA interface. At times, the VISAR signal degraded quickly, in some cases from abrasion of the vapor-deposited aluminum layer on the PMMA window. Thicker aluminum layers were used more successfully. In conjunction, these two techniques allow us to make redundant measurements of particle velocity which improves experimental uncertainties.

2.4. Further Experimental Considerations

Our experimental analysis relies on the assumption that our measurements are being made under uniaxial compression. However, this is only true within a certain spatial and temporal regime in the experiment. The goal of this analysis will be to show that with 1σ uncertainty, all measurements are made under uniaxial compression.

At the outer diameter of the soil sample, there is an impedance mismatch between the polycarbonate capsule and the soil which will cause lateral release waves to propogate

radially inward towards the center of the sample. The leading edge of these waves will propogate at the bulk sound velocity in the shock state of the soil, given by:

$$c_b^2 = \left(\frac{\partial P}{\partial \rho}\right)_S$$

Using a Mie-Grüneisen equation of state, we can use the known Hugoniot of the soils, calculated from the impedance match, to approximate this derivative [Duffy and Ahrens, 1992].

$$c_b = \left\{\left(\frac{\partial P}{\partial \rho}\right)_H \left[1 - \left(\frac{1}{\rho_0} - \frac{1}{\rho}\right)\frac{\rho\gamma}{2}\right] + \frac{P_H\gamma}{2\rho}\right\}^{\frac{1}{2}} \tag{1}$$

Since we are taking our measurements at the back surface of the target, we use expression for the diameter on the rear surface where the compression is still uniaxial, derived by [Swift and Kraus, 2008]:

$$d_1 = d_0 - 2l_0\tan\Phi \tag{2}$$

where d_1 is the region not affected by lateral release, d_0 is the outer diameter of the target, and l_0 is the thickness of the target, and Φ is the release angle, given by:

$$\Phi = \tan^{-1}\left[\left(\frac{c_b^2 - (U_s - u_p)^2}{U_s^2}\right)^{\frac{1}{2}}\right] \tag{3}$$

Using the Hugoniot of the soil measured by the impedance match calculation and a Mie-Grüneisen parameter of 1.2±0.3, d_1 is plotted in Figures 2-5 as a function of shock velocity for both the dry and wet VIMF. Error bars are generated using the Taylor series method discussed in Section 3.3.3.

3. Results
3.1. Shock Hugoniot States

Given an initial thermodynamic state, the Rankine-Hugoniot conservation equations govern the locus of thermodynamic states that are attainable by a single shock process. These relations require the conservation of mass, momentum and energy across a shock front and are given by:

$$u_{p1} - u_{p0} = U_s\left(1 - \frac{V_1}{V_0}\right) \tag{4}$$

$$P_1 - P_0 = \frac{U_s}{V_0}(u_{p1} - u_{p0}) \tag{5}$$

$$E_1 - E_0 = \frac{1}{2}(P_1 - P_0)(V_0 - V_1) \tag{6}$$

In the above equations, the 0 subscripts denote the unshocked state and the 1 subscripts denote the shocked state. In our experimental setup, the initial particle velocity is zero

and the initial pressure is approximately zero. The initial specific volume, V_0 is calculated by careful measurement of the mass and volume of a sample element. Thus, to fully constrain the problem and find the relationship between P, V, and E on the Hugoniot we need to experimentally measure the relationship between the shock velocity, U_s, and the particle velocity, u_{p1}.

3.1.1. Impedance Match Method

For the purposes of this analysis, parameters relating to the aluminum driver, the soil sample, and the PMMA window will be denoted by the subscripts a, b, and c, respectively. At time t=0, the aluminum flyer impacts the driver generating a shock wave which excites a particle velocity of $-\frac{1}{2}$ the flyer velocity and $\frac{1}{2}$ the flyer velocity in the flyer and driver respectively. When the shock wave reaches the driver/soil interface, there is a partial release of pressure along the driver's isentrope due to the lower impedance of the soil. We assume that this isentrope is well approximated by the principal Hugoniot of aluminum reflected about the axis in $P - u_p$ space where the particle velocity is equal to $\frac{1}{2}$ the flyer velocity. This is generally a good assumption in the relatively low pressure regime attained in these experiments. Using both piezoelectric pins and a velocity interferometry system for any reflector (VISAR) as separate non-correlated measurements, we find the time at which the shock wave reaches the driver/soil interface. Similarly, we measure the time at which the shock wave reaches the soil/PMMA interface. This allows us to measure the transit time of the shock through the soil sample. By measuring the sample thickness prior to the shock experiment, we are able to calculate the shock velocity in the soil. Shock velocities are made more accurate by applying a flyer plate tilt correction which accounts for the deviation of the plane of the driver from the plane of the projectile.

The corresponding particle velocity is obtained using two separate methods. The first is an impedance matching method, which requires that the driver release to the state that intersects the Rayleigh line of the soil (Figure 6). From Equation 5, the Hugoniot of aluminum in the $P - u_p$ plane is:

$$P = \rho_a U_{sa} u_{pb1}$$

From experimental data previously collected on aluminum, we know that there is a linear relationship between particle velocity and shock velocity within our experimental domain. Plugging in $U_s = C_a + S_a u_p$, where C_a is an experimentally measured value related to the bulk sound speed of aluminum, and S_a is an experimentally measured constant, we can rewrite our expression for the Hugoniot of aluminum:

$$P = \rho_a(C_a + S_a u_{pb1}) u_{pb1}$$

If we assume release along the reflected Hugoniot of aluminum, then the expression for the release path is:

$$P = \rho_a[C_a + S_a(V_f - u_{pb1})](V_f - u_{pb1})$$

The impedance match constraint tells us that:

$$\rho_a[C_a + S_a(V_f - u_{pb1})](V_f - u_p) = \rho_b U_{sb} u_{pb1}$$

Solving for u_{pb1}, we find that:

$$u_{pb1} = \frac{C_a\rho_a + 2S_a v_f \rho_a + U_{sb}\rho_b + \sqrt{C_a^2\rho_a^2 + 2C_a U_{sb}\rho_a\rho_b + 4S_a U_{sb} v_f \rho_a\rho_b + U_{sb}^2\rho_b^2}}{2S_a\rho_b} \quad (7)$$

Aluminum 2024 was chosen as a flyer and driver because its shock properties are well characterized, which reduces the uncertainty in the impedance match calculation (by minimizing the uncertainty in the driver Hugoniot parameters C_a and S_a). Additionally, the impedance of aluminum is a better match to the impedance of our samples than other common impactors such as steel, which minimizes the uncertainty due to the assumption that the isentrope of the driver is well approximated by the Hugoniot. We use the data in Marsh [1980] with $u_p < 900$ m s^{-1} to fit an aluminum 2024 Hugoniot in the pressure range of interest: $U_S = 5.362 + 1.3026 u_p$. Using the impedance match method, we found the following $U_s - u_p$ relations:

$$u_{S1} = \begin{cases} 0.5270 + 2.1545 u_{pb1} & \text{Dry VIMF} \\ 0.3249 + 2.6445 u_{pb1} & \text{Dry ATC Sand-Clay} \\ 0.3050 + 2.3226 u_{pb1} & \text{Dry ATC DSTS} \\ 2.0818 + 2.1464 u_{pb1} & \text{Wet VIMF} \\ 2.1962 + 1.5135 u_{pb1} & \text{Wet ATC Sand-Clay} \\ 2.3583 + 2.3608 u_{pb1} & \text{Wet ATC DSTS} \end{cases} \quad (8)$$

where the fit parameters had the correlation coefficients:

$$\rho_1 = \begin{cases} -0.960 & \text{Dry VIMF} \\ -0.935 & \text{Dry ATC Sand-Clay} \\ -0.914 & \text{Dry ATC DSTS} \\ -0.938 & \text{Wet VIMF} \\ -0.956 & \text{Wet ATC Sand-Clay} \\ -0.939 & \text{Wet ATC DSTS} \end{cases} \quad (9)$$

3.2. VISAR method

Using a VISAR, we can directly measure the particle velocity at the soil sample/ PMMA interface, which is a state on the Hugoniot of PMMA and the release isentrope of the

soil. To find the particle velocity in the shock state of the soil, we need to know both the Hugoniot of PMMA (shown in red in Figure 6) as well as an expression for the isentropic pressure release path from the soil to the PMMA (shown in green in Figure 6). To determine the Hugoniot of PMMA, we used a cubic fit to the dataset published by [Marsh, 1980] at relevant particle velocities ($u_p < 1$ km s^{-1}).

$$U_c = C_c + S_c u_p + S'_c up^2 + S''_c up^3 \tag{10}$$

Where $C_c = 2.8$, $S_c = 2.1$, $S'_c = -2.9$, and $S''_c = 2.1$. In $P - u_p$ space, the general expression for the Hugoniot of PMMA can be written as:

$$P_{Hc} = \rho_c U_{sc} u_p = \rho_c (C_c + S_c u_p + S'_c up^2 + S''_c up^3) u_p \tag{11}$$

Next, we assume that the isentropic release is well approximated by the reflected Hugoniot of the soil. We use the $U_s - u_p$ relation calculated from the impedance match method to make this correction. This means that the particle velocity measured from the VISAR method is not completely uncorrelated from the impedance match method. However, the particle velocity correction due to the impedance mismatch between the soil and the PMMA is small relative to the total particle velocity, so we treat the particle velocity measured from the VISAR method as approximately uncorrelated to the particle velocity measured from the impedance match method. From the impedance match data, we see that the Hugoniot of the soil is well fit by a line, so the Hugoniot of the soil is:

$$P_{Hb} = \rho_b (C_b + S_b u_p) u_p \tag{12}$$

So the expression for the approximate isentrope is:

$$P_{Sb} \approx \rho_b [C_b + S_b (2u_{pb2} - u_p)](2u_{pb2} - u_p) \tag{13}$$

Where u_{pb} is the axis of reflection, which is equal to the particle velocity in the shock state of the soil. By the impedance match criterion, we know that the pressure on the isentrope of the soil must be equal to the pressure on the Hugoniot of the PMMA:

$$P_{Hc} = P_{Sb} \tag{14}$$

Plugging Equation 11 and 13 in to 14 and solving for u_{pb2}, we get the following expression for the particle velocity in the shock state of the soil sample as a function of the measured particle velocity and the Hugoniot parameters of the soil sample and PMMA:

$$u_{pb2} = \frac{-C_b \rho_b + 2S_b \rho_b u_p + \sqrt{\rho_b (C_b^2 \rho_b + 4S_b u_p (C_c + u_p (S_c + u_p (S'_c + S''_c u_p))) \rho_c)}}{4S_b \rho_b} \tag{15}$$

Using the VISAR technique, we calculated the following $U_s - u_p$ relations:

$$u_{S2} = \left\{ \; 2.5863 + 1.6950 u_{pb2} \; \text{ Wet ATC-DSTS} \right. \tag{16}$$

with correlation coefficient:

$$\rho_2 = \left\{ \; -0.934 \; \text{ Wet ATC-DSTS} \right. \tag{17}$$

3.3. Shock Hugoniot Uncertainties

Due to the limited number of experiments we were able to conduct for each soil sample, a rigorous quantification of experimental uncertainties was done. The goals of this analysis are to:

1. Relate the uncertainties in the measured parameters to the uncertainties in the calculated Hugoniot parameters from Equations 4, 5, 7, and 15.

2. Demonstrate that the VISAR Hugoniot parameters are approximately independent of the impedance match Hugoniot parameters.

3. Define the important experimental parameters, to serve as a way to reduce uncertainties in future plate impact experiments.

4. Relate the uncertainties in the experimental Hugoniot parameters to the uncertainties in the equation of state variables (the coefficients of the $U_s - u_p$ relation).

The data shown in Tables 3-8 are presented as unique measurements with 1-dimensional uncorrelated uncertainties. In reality, the uncertainties in each calculated parameter are correlated and fall an an ellipse in n-dimensional space, where n is the number of calculated parameters. The following analysis presents the variance and covariance of our experimental calculations.

3.3.1. Measurement Uncertainties

1. Uncertainties in shock arrival times are taken to be 75% of the signal rise time on the upper end and 25% of the signal rise time on the lower end for both the VISAR and the piezoelectric pins. The shock breakout time is taken to be 50% of the signal rise time. Uncertainties in the shock arrival times are generally on the order of ~10 ns.

2. Uncertainties in the sample density are calculated using the published accuracies of our micrometer and scale. Taking several repeated measurement helps to increase the precision of our density calculation.

3. Uncertainties in the flyer velocity are taken to be 75% and 25% of the voltage drop caused by the flyer interrupting the laser beam lines. The flyer arrival time is taken to be 50% of the voltage drop.

3.3.2. Hugoniot Uncertainties

Let $f_n(x_1, ..., x_i)$ be a set of k linearly independent functions of i variables ($n = 1, ..., k$). We have $k = 6$ functions corresponding to Equations 4, 5, 7, 15 and $i = 14$ unique variables. Given the variance-covariance matrix of the independent variables denoted $\mathbf{\Sigma_x}$, the goal is to find the variance-covariance matrix of the dependent variables $\mathbf{\Sigma_f}$, which will give us both the uncertainties in our calculated parameters as well as the strength of the correlation between the values calculated from the impedance match and those calculated from the VISAR. This is used to justify presenting each method as a unique measurement. We developed two approaches to the problem. First we will use an analytical solution using a first order Taylor approximation, which allows us to quantify the error contribution from each measurement to the total uncertainty in the Hugoniot parameters. Second we employ a Monte Carlo technique that generates a numerical solution to check the validity of the analytical approach.

3.3.3. Taylor Series Method

Consider the set of vector valued functions:

$$f_n = f_n(x_1, x_2, ..., x_i) \tag{18}$$

where f_n are the set of experimental results determined from i measured variables x_i. Each of the measurements has a total uncertainty which is equal to the difference between the true value of the variable and the measurement value. The total uncertainty can be decomposed into both random and systematic components, denoted in the following way:

$$\underbrace{\bar{x}_i}_{\text{measured}} = \underbrace{x_i}_{\text{true}} + \underbrace{sx_i}_{\text{sys error}} + \underbrace{ex_i}_{\text{rand error}} \tag{19}$$

Next we approximate the set of functions f_n by Taylor expansion:

$$\bar{f}_n = f_n + \frac{\partial f_n}{\partial x_i}(\bar{x}_i - x_i) + O^2 \tag{20}$$

We can rewrite this in terms of the random and systematic errors:

$$\sigma f_n \approx \frac{\partial f_n}{\partial x_i}|_{\bar{x}_i}(sx_i + ex_i)$$

There are two fundamental assumptions associated with Equation 20. The first assumption is that the higher order terms are negligible, which is reasonable when the measurement error is small since the next term in the series expansion contains the square of the measurement errors. This assumption is is verified by the Monte Carlo analysis. The second assumption is that the derivative of f_n evaluated at $\bar{x}_i$ is a good approximation of the derivative of f_n at x_i, which cannot be rectified by the Monte Carlo analysis, since we dont know the values of x_i.

We are interested in seeing how the distribution of errors in x_i maps to the distribution of errors in f_n, so square both sides of the equation to find the variance of the distribution about f_n. We assume that the systematic errors will be small compared to the random errors, so we set ex_i to 0. However, from this analysis, we can look at the prefactor of each of the systematic error terms to understand how much a systematic error in the variable x_i will affect the uncertainty in f_n.

$$\sigma^2 f_n = \left(\frac{\partial f_n}{\partial x_i} s x_i\right)^2$$

$$\sigma^2 f_n = \frac{\partial f_n}{\partial x_i} s x_i s x_j \frac{\partial f_n}{\partial x_j} \tag{21}$$

Where $\frac{\partial f_n}{\partial x_j}$ is the transpose of $\frac{\partial f_n}{\partial x_i}$. This gives us the desired result in index notation. Notice that $\frac{\partial f_n}{\partial x_i}$ is just the jacobian of f_n, so we can write this result in matrix form:

$$\mathbf{\Sigma_f}^{\text{Tay}} = \mathbf{J} \mathbf{\Sigma_x} \mathbf{J^T} \tag{22}$$

3.3.4. Monte Carlo method

Here we take a numerical approach to the same problem. In addition to the value of each measurement, $\bar{x}_i$, we know the covariance matrix $\mathbf{\Sigma_x}$, as discussed in Section 3.3.1. We use this information to generate random points from a multivariate normal distribution. This gives us an array of observations of f_n, denoted f_{nk} (the kth observation of the parameter f_n. From this set of points, we calculate the covariance matrix of f_n:

$$\mathbf{\Sigma_f}^{\text{MC}} = \frac{1}{k-1} \sum_i^k (f_{ij} - \bar{f}_j)(f_{ik} - \bar{f}_k)$$

For large enough n, $\mathbf{\Sigma_f}^{\text{MC}}$ converges to the true value of $\mathbf{\Sigma_f}$ provided that there are no systematic errors which are unaccounted for in the input covariance matrix $\mathbf{\Sigma_x}$.

3.3.5. Discussion

We have confirmed that the covariance matrix calculated from the Taylor series method is in good agreement with the covariance matrix calculated from the Monte Carlo method. In this paper, we present the uncertainties calculated from the Taylor series approach, as the analytical method allowed us to decompose the total uncertainty in f_n into its component uncertainties from the variables x_i which helped to verify that the propagated uncertainties made sense.

We see that the parameters calculated from the impedance match technique are independent of those from the VISAR technique. This is as expected since the impedance match calculations relied only on independent measurements. However, the uncertainties

in the parameters calculated from the VISAR technique are correlated to the those of the impedance match technique through the Hugoniot parameters C_s and S_s calculated from the impedance match technique. To evaluate the strength of the linear correlation between the particle velocity from the impedance match (up_1) and the particle velocity calculated from the VISAR technique (up_2), we use the Pearson product-moment correlation coefficient, which gives values between -1 and 1, where a value of 0 is no correlation between the two variables. The correlation coefficient is defined as:

$$\rho_{x,y} = \frac{\text{cov}(x,y)}{\sigma_x \sigma_y}$$

As shown in the example calculation, the correlation coefficient between u_{pb1} and u_{pb2} is on the order of ~ 0.001, which implies that the variables are approximately independent. This justifies treating each as an independent measurement.

3.3.6. Hugoniot Linear Fit Uncertainties

The linear fits to the $U_s - u_p$ data are calculated using the weighted total least squares method described by [Krystek and Anton, 2007], which fits a straight line to data with uncertainties in both the independent (u_p) and dependent (U_s) variables. This method also allows us to generate the covariance matrix for the fit parameters shown here.

$$\text{Dry VIMF 1}: \begin{bmatrix} 0.0006 & -0.0085 \\ -0.0085 & 0.0014 \end{bmatrix} \tag{23}$$

$$\text{Dry ATC-SandClay 1}: \begin{bmatrix} 0.0011 & -0.0017 \\ -0.0017 & 0.0033 \end{bmatrix} \tag{24}$$

$$\text{Dry ATC-DSTS 1}: \begin{bmatrix} 0.0002 & -0.0003 \\ -0.0003 & 0.0006 \end{bmatrix} \tag{25}$$

$$\text{Wet VIMF 1}: \begin{bmatrix} 0.0121 & -0.0204 \\ -0.0204 & 0.0391 \end{bmatrix} \tag{26}$$

$$\text{Wet ATC-SandClay 1}: \begin{bmatrix} 0.0057 & -0.0092 \\ -0.0092 & 0.0163 \end{bmatrix} \tag{27}$$

$$\text{Wet ATC-DSTS 1}: \begin{bmatrix} 0.0019 & -0.0036 \\ -0.0036 & 0.0080 \end{bmatrix} \tag{28}$$

$$\text{Wet ATC-DSTS 2}: \begin{bmatrix} 0.0671 & -0.1286 \\ -0.1286 & 0.0671 \end{bmatrix} \tag{29}$$

$$\tag{30}$$

3.4. Summary of Hugoniot Measurements

The measured Hugoniot states for each soil are presented in Figures 7-12 and Tables 3-8.

4. Discussion and future work

In all cases, water-saturated soils have a larger shock velocity and higher impedance compared to the dry samples. The wet soil Hugoniot data are in excellent agreement with the ice-saturated quartz sand data from Kraus et al. [2010]. However, we found considerable scatter in water-saturated samples. The scatter was more pronounced in singly-pressed samples (primarily ATC Sand-Clay). Subsequently, multiply-pressed samples significantly reduced the scatter bewteen the different measurement techniques on a single sample. In one experiment, a water-saturated sample had the water pumped out in the target chamber immediately before the experiment. This experiment had a shock velocity nearly identical to the dry sample. A survey of the literature finds considerable scatter in wet soil or sand samples. In some cases, the wet shock velocity is very close to the dry shock velocity (e.g., Chapman et al. [2006]), and we suggest that water loss may have occurred in these cases. We added a capacitance sensor to the wet target configuration to check for water loss in the following experiments.

Detailed simulations of the wave propagation through the dry and wet soils for comparison to the VISAR data records is ongoing. In Figure 13, the particle velocities measured in the final shock state display a characteristic 'ringing' pattern. Based on our ongoing simulations using the CTH shock physics code, the ringing arises from wave reflections between the grains. Further analyses of these data will improve the modeling of heterogeneous granular materials (e.g., Vogler et al. [2010]).

5. Presentations

Kraus, R. G., M. G. Newman, S. T. Stewart, Hugoniot Measurements on Heterogeneous Geologic Materials, Lunar and Planetary Science Conference 43, 2680, 2012.

Newman, M., S. T. Stewart, R. G. Kraus, Hugoniot Measurements on Dry and Water-Saturated Soils, American Geophysical Union Fall Meeting, Abs. P11A-1788, 2012.

Journal paper in preparation: Newman, M. G., S. T. Stewart, R. G. Kraus, Hugoniot Measurements on Dry and Water-Saturated Soils, Journal of Geophysical Research.

References

Barker, L. M., Hollenbach, R. E., 1972. Laser interferometer for measuring high velocities of any reflecting surface. Journal of Applied Physics 43, 4669–4675, DOI:10.1063/1.1660986.

Chapman, D., Tsembelis, K., Proud, W., 2006. The behaviour of water saturated sand under shock-loading. In Proc. 2006 SEM Ann. Conf. and Exposition on Experimental and Applied Mechanics, Society for Experimental Mechanics, Bethel CT, p. paper 400.

Duffy, T., Ahrens, T., 1992. Sound velocities at high pressure and temperature and their geophysical implications. Journal of Geophysical Research 97 (B4), 4503–4520.

Kraus, R. G., Stewart, S. T., Seifter, A., Obst, A. W., 2010. Shock and post-shock temperatures in an ice-quartz mixture: implications for melting during planetary impact events. Earth Planet. Sci. Lett. 289 (1-2), 162–170, DOI:10.1016/j.epsl.2009.11.002.

Krystek, M., Anton, M., 2007. A weighted total least-squares algorithm for fitting a straight line. Measurement Science and Technology 18 (11), 3438.

Marsh, S. P., 1980. LASL Shock Hugoniot Data. University of California Press, Berkeley, California.

Swift, D.-C., Kraus, R.-G., 2008. On the properties of plastic ablators in laser-driven material dynamics experiments. Phys. Rev. E 77, 066402.

Vogler, T., Alexander, C., Wise, J., Montgomery, S., 2010. Dynamic behavior of tungsten carbide and alumina filled epoxy composites. Journal of Applied Physics 107 (4), 043520–043520–13.

Table 1.   Mineral abundances (wt %). Quartz, kaolinite, muscovite and hematite were identified in each of the clays using x-ray diffraction.   Amorphous materials may include amorphous silica, Fe oxyhydroxides, and poorly crystalline or amorphous clays.

Soil	Name	Quartz	Kaolinite	Muscovite	Hematite	Amorphous
1	VIMF	60.4	13.2	5.1	0.3	21.0
2	ATC Sand-Clay	67.2	16.4	7.2	0.2	9.0
3	ATC-DSTS	56.5	1.0	11.0	0.5	31.0

Table 2.   Soil characteristics.

| Soil	Name	Crystal density (g/cm^3)	Dry bulk density (g/cm^3)	Porosity	Water-saturated bulk density (g/cm^3)
1	VIMF	2.539	1.843	0.274	2.231
2	ATC Sand-Clay	2.566	1.914	0.254	2.331
3	ATC-DSTS	2.548	1.750	0.313	2.297
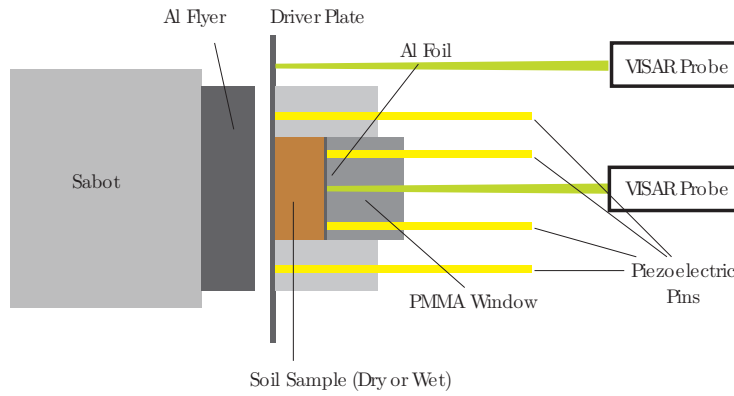
Figure 1. Target schematic (side view) for determining the Hugoniot state via measurement of the shock wave transit time. The VISAR is used to determine if any corrections need to be made for a multi-wave structure. The soil experiments utilized simultaneous piezoelectric pins and VISAR at 2 to 5 points on the sample.
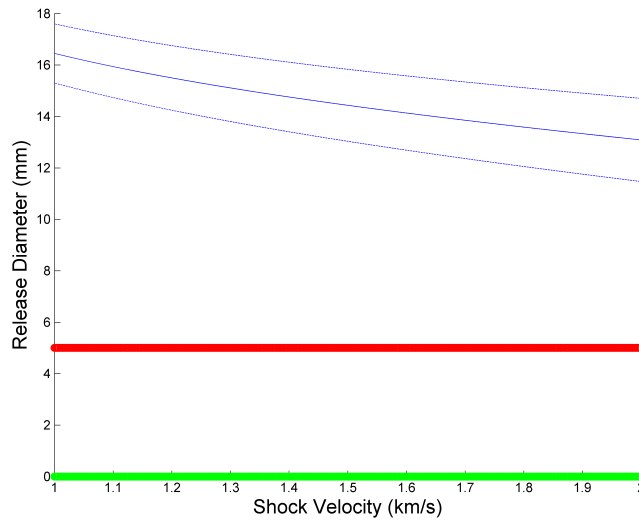

Figure 2. The diameter over which the experiment remains one dimensional with 1-σ error as a function of shock velocity for the dry soil. The location of the pins and the visar are shown in red and green respectively.
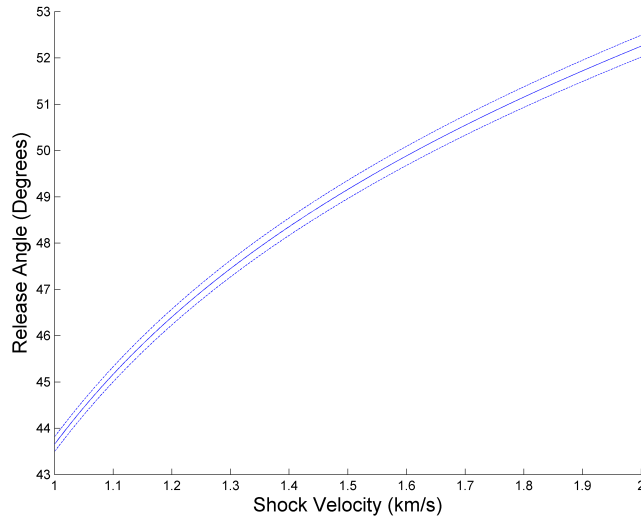
Figure 3.   Release angle as a function of shock velocity with 1-σ error over the relevant experimental domain for the dry soil.
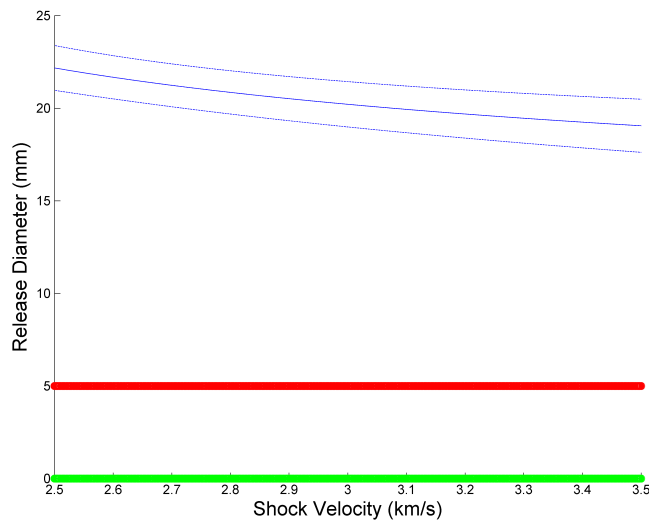
Figure 4.   The diameter over which the experiment remains one dimensional with 1-σ error as a function of shock velocity for the wet soil. The location of the pins and the visar are shown in red and green respectively.
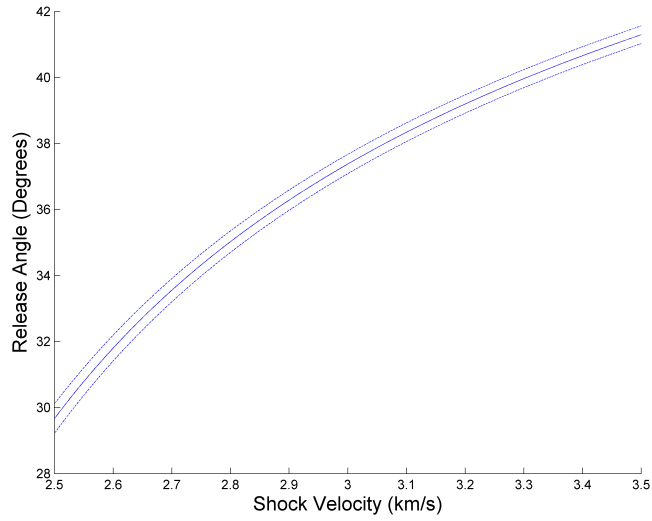
Figure 5. Release angle as a function of shock velocity with 1-σ error over the relevant experimental domain for the wet soil.
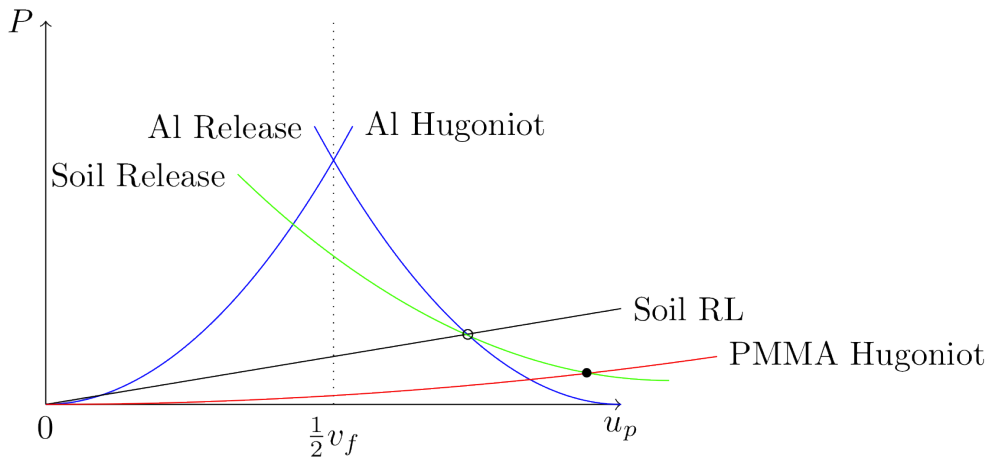

Figure 6. Summary of Hugoniot measurements using two methods. The open circle represents the value calculated by the impedance match method and the closed circle represents the value measured directly by the VISAR.
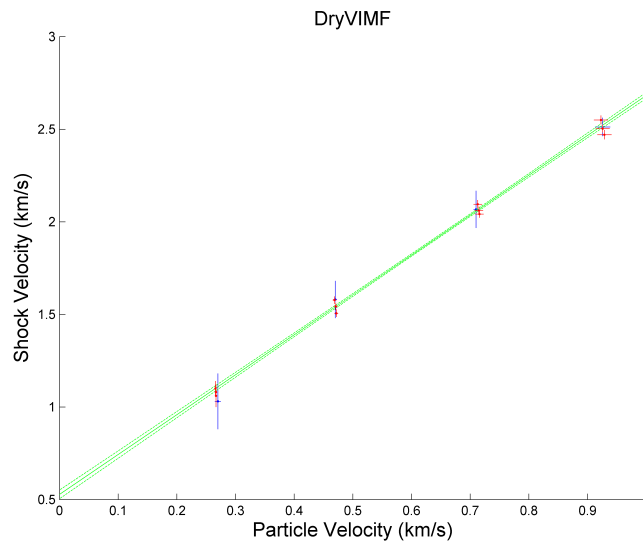
Figure 7. Principal Hugoniot of the dry VIMF. Points shown in red are collected from the pin impedance match and points shown in blue are collected from the VISAR impedance match. Error bars are 1-σ calculated from the Taylor series method.
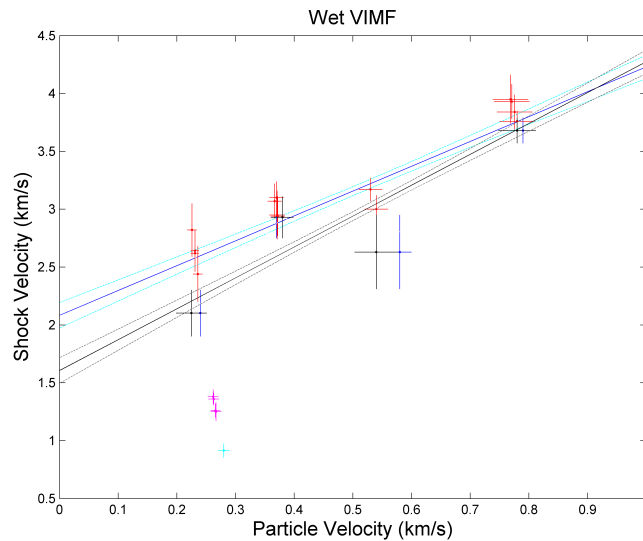
Figure 8. Principal Hugoniot of the wet VIMF. Points shown in red are collected from the pin impedance match, points shown in blue are collected from the VISAR impedance match, and points shown in black are collected from the VISAR wave profile. Error bars are 1-σ calculated from the Taylor series method. The points shown in pink and light blue fall on the dry VIMF hugoniot, indicating that the sample lost water before the shot.
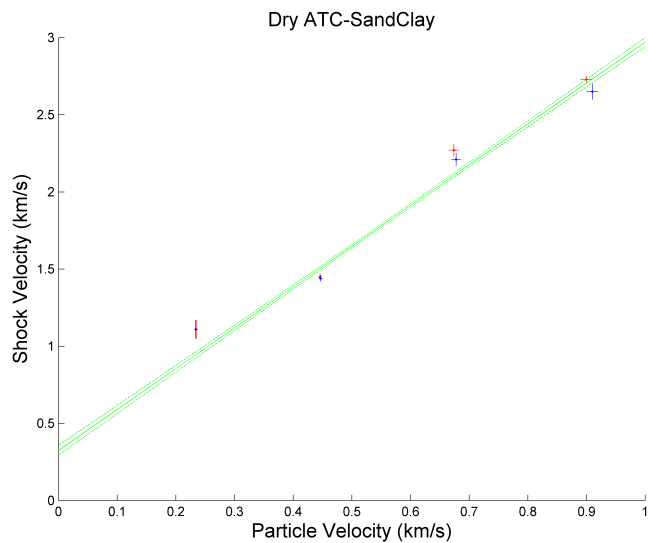
Figure 9.   Principal Hugoniot of the dry ATC Sand-Clay.
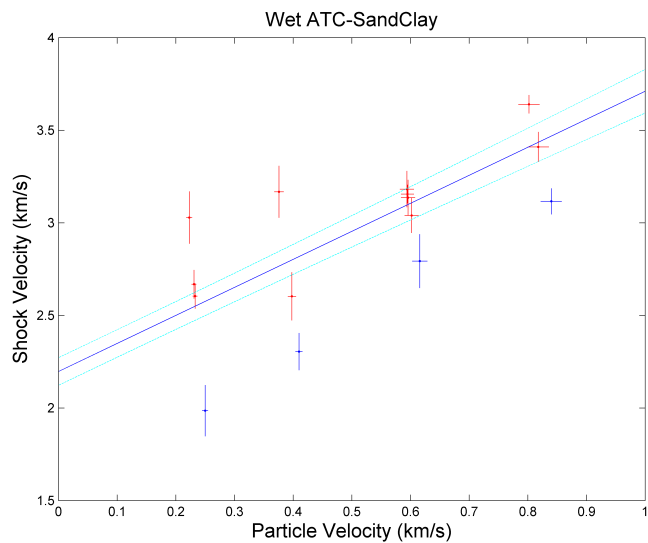
Figure 10.   Principal Hugoniot of the wet ATC Sand-Clay.
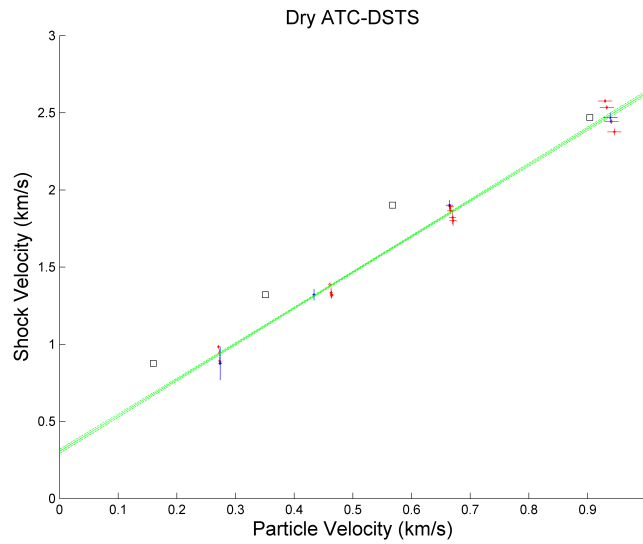
Figure 11. Principal Hugoniot of the dry ATC DSTS. The systematic lower particle velocity measured from the VISAR wave profile (shown as black squares) compared to the impedance match (shown in blue for the VISAR and red for the pins), suggests stress relaxation after the initial shock.
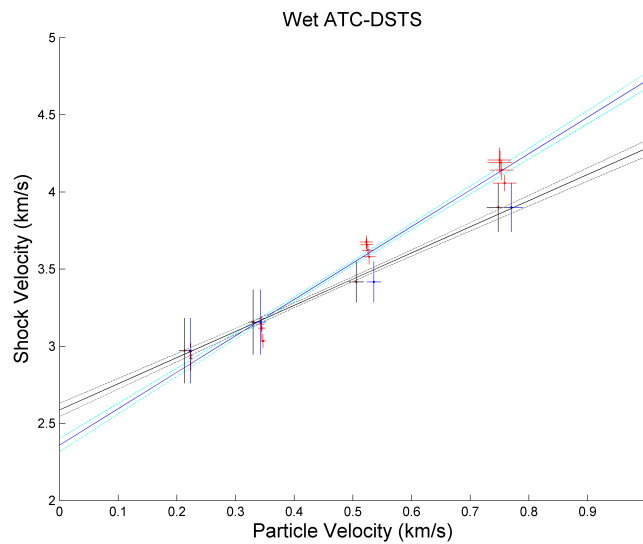
Figure 12. Principal Hugoniot of the wet ATC DSTS. The fit to the VISAR data is shown in black and the fit to the impedance match data is shown in blue.
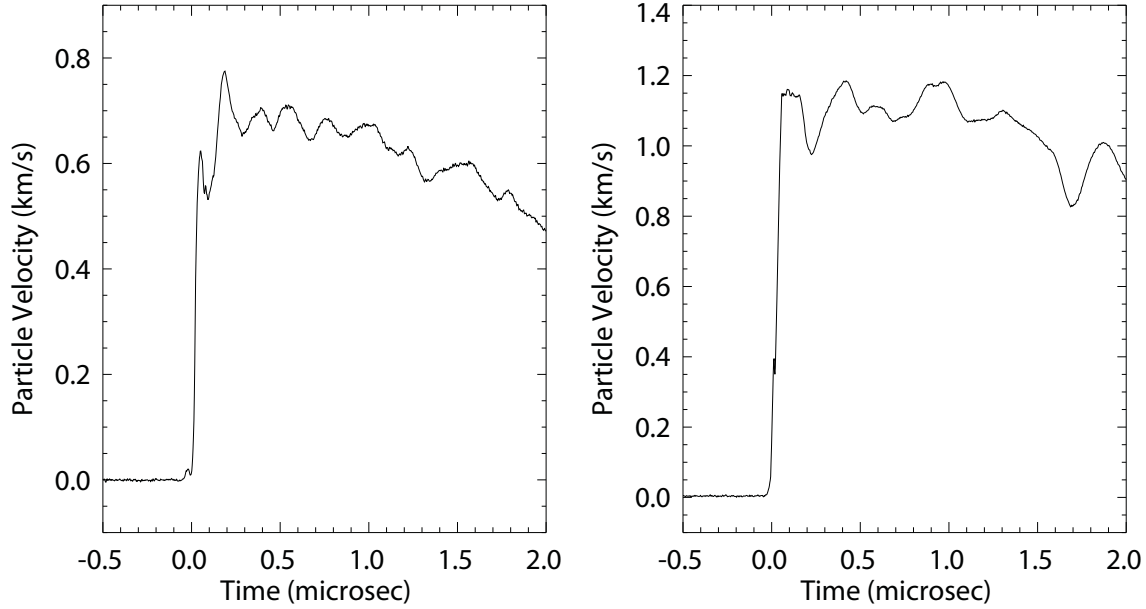
Figure 13.   Examples of VISAR wave profiles at the water-saturated VIMF soil-PMMA interface. Impact velocities were 528 and 796 m/s. The 'ringing' at the top of the wave arises from pressure variations in the heterogeneous sample.

Table 3.   Dry VIMF Impedance Match Data

| Shot	Measurement	U_s	u_p	P	ν
099	VISAR	$2.51 \pm .04$	$0.93 \pm .01$	$4.23 \pm .09$	$0.348 \pm .006$
	J	$2.55 \pm .02$	$0.92 \pm .01$	$4.27 \pm .07$	$0.351 \pm .004$
	K	$2.50 \pm .02$	$0.93 \pm .01$	$4.21 \pm .06$	$0.347 \pm .004$
	L	$2.47 \pm .03$	$0.93 \pm .01$	$4.17 \pm .07$	$0.343 \pm .004$
098	VISAR	$2.07 \pm .05$	$0.710 \pm .004$	$2.68 \pm .05$	$0.360 \pm .006$
	I	$2.10 \pm .02$	$0.713 \pm .007$	$2.71 \pm .04$	$0.360 \pm .003$
	J	$2.10 \pm .02$	$0.713 \pm .007$	$2.71 \pm .04$	$0.360 \pm .004$
	K	$2.04 \pm .02$	$0.716 \pm .007$	$2.65 \pm .04$	$0.358 \pm .004$
	L	$2.06 \pm .02$	$0.715 \pm .007$	$2.67 \pm .04$	$0.360 \pm .003$
101	VISAR	$1.58 \pm .05$	$0.470 \pm .003$	$1.38 \pm .04$	$0.380 \pm .006$
	I	$1.54 \pm .02$	$0.471 \pm .003$	$1.35 \pm .02$	$0.373 \pm .003$
	J	$1.58 \pm .02$	$0.469 \pm .003$	$1.38 \pm .02$	$0.377 \pm .003$
	K	$1.54 \pm .02$	$0.471 \pm .003$	$1.35 \pm .02$	$0.373 \pm .003$
	L	$1.51 \pm .02$	$0.472 \pm .003$	$1.33 \pm .02$	$0.368 \pm .003$
102	VISAR	$1.03 \pm .03$	$0.270 \pm .005$	$0.52 \pm .07$	$0.39 \pm .02$
	I	$1.08 \pm .04$	$0.267 \pm .002$	$0.54 \pm .02$	$0.401 \pm .006$
	J	$1.10 \pm .04$	$0.266 \pm .002$	$0.55 \pm .02$	$0.404 \pm .006$
	L	$1.06 \pm .06$	$0.267 \pm .002$	$0.53 \pm .03$	$0.398 \pm .009$

Table 4. Wet VIMF Impedance Match Data

Shot	Measurement	U_s	u_p	P	ν
110	VISAR	$2.10 \pm .2$	$0.24 \pm .01$	$1.16 \pm .11$	$0.39 \pm .03$
	I	$2.82 \pm .23$	$0.226 \pm .008$	$1.44 \pm .12$	$0.41 \pm .03$
	J	$2.64 \pm .18$	$0.231 \pm .007$	$1.38 \pm .11$	$0.40 \pm .03$
	K	$2.44 \pm .24$	$0.236 \pm .008$	$1.30 \pm .12$	$0.40 \pm .03$
	L	$2.62 \pm .16$	$0.231 \pm .007$	$1.37 \pm .10$	$0.40 \pm .03$
103	VISAR	$3.68 \pm .11$	$0.79 \pm .02$	$6.43 \pm .40$	$0.35 \pm .03$
	I	$3.76 \pm .09$	$0.78 \pm .03$	$6.52 \pm .42$	$0.36 \pm .03$
	J	$3.84 \pm .15$	$0.78 \pm .03$	$6.62 \pm .45$	$0.36 \pm .03$
	K	$3.93 \pm .15$	$0.77 \pm .03$	$6.72 \pm .45$	$0.36 \pm .03$
	L	$3.95 \pm .21$	$0.77 \pm .03$	$6.75 \pm .49$	$0.36 \pm .03$
105	VISAR	$2.93 \pm .18$	$0.37 \pm .01$	$2.41 \pm .19$	$0.39 \pm .03$
	I	$3.10 \pm .14$	$0.37 \pm .012$	$2.51 \pm .17$	$0.40 \pm .03$
	J	$3.07 \pm .15$	$0.37 \pm .012$	$2.50 \pm .18$	$0.40 \pm .03$
	K	$2.95 \pm .21$	$0.37 \pm .013$	$2.43 \pm .20$	$0.40 \pm .03$
	L	$2.94 \pm .17$	$0.37 \pm .012$	$2.42 \pm .18$	$0.40 \pm .03$
104	VISAR	$2.63 \pm .32$	$0.58 \pm .02$	$3.37 \pm .37$	$0.35 \pm .03$
	J	$3.17 \pm .10$	$0.53 \pm .02$	$3.71 \pm .25$	$0.37 \pm .03$
	L	$3.00 \pm .12$	$0.54 \pm .02$	$3.57 \pm .25$	$0.37 \pm .03$
106*	VISAR	$0.92 \pm .06$	$0.28 \pm .01$	$0.56 \pm .09$	$0.31 \pm .05$
	I	$1.36 \pm .05$	$0.263 \pm .009$	$0.79 \pm .12$	$0.36 \pm .06$
	J	$1.38 \pm .06$	$0.262 \pm .009$	$0.80 \pm .12$	$0.37 \pm .06$
	K	$1.25 \pm .08$	$0.267 \pm .009$	$0.74 \pm .11$	$0.36 \pm .06$
	L	$1.26 \pm .06$	$0.266 \pm .008$	$0.75 \pm .11$	$0.36 \pm .06$

Table 5. Dry ATC Sand-Clay Impedance Match Data

Shot	Measurement	U_s	u_p	P	ν
092	VISAR	$1.11 \pm .06$	$0.234 \pm .002$	$0.50 \pm .02$	$0.409 \pm .008$
	Pin	$1.10 \pm .04$	$0.235 \pm .002$	$0.50 \pm .02$	$0.408 \pm .006$
114	VISAR	$1.34 \pm .03$	$0.463 \pm .003$	$1.07 \pm .02$	$0.379 \pm .005$
	I	$1.32 \pm .02$	$0.464 \pm .003$	$1.06 \pm .02$	$0.375 \pm .004$
	J	$1.33 \pm .03$	$0.463 \pm .003$	$1.07 \pm .02$	$0.377 \pm .005$
	K	$1.32 \pm .03$	$0.464 \pm .003$	$1.06 \pm .02$	$0.375 \pm .005$
	L	$1.39 \pm .03$	$0.460 \pm .003$	$1.11 \pm .02$	$0.388 \pm .005$
091	VISAR	$1.44 \pm .02$	$0.447 \pm .003$	$1.22 \pm .02$	$0.365 \pm .003$
	Pin	$1.45 \pm .02$	$0.446 \pm .003$	$1.22 \pm .02$	$0.367 \pm .004$
088	VISAR	$2.21 \pm .04$	$0.678 \pm .008$	$2.88 \pm .06$	$0.360 \pm .005$
	Pin	$2.27 \pm .04$	$0.674 \pm .008$	$2.95 \pm .05$	$0.365 \pm .004$
087	VISAR	$2.65 \pm .05$	$0.91 \pm .01$	$4.59 \pm .09$	$0.344 \pm .005$
	Pin	$2.73 \pm .02$	$0.90 \pm .01$	$4.70 \pm .08$	$0.350 \pm .003$

Table 6. Wet ATC Sand-Clay Impedance Match Data

Shot	Measurement	U_s	u_p	P	ν
109	VISAR	$1.99 \pm .13$	$0.250 \pm .005$	$1.16 \pm .06$	$0.375 \pm .005$
	J	$3.03 \pm .14$	$0.223 \pm .005$	$1.57 \pm .06$	$0.397 \pm .003$
	K	$2.67 \pm .08$	$0.231 \pm .004$	$1.44 \pm .04$	$0.392 \pm .002$
	L	$2.604 \pm .07$	$0.233 \pm .004$	$1.42 \pm .03$	$0.391 \pm .002$
095	VISAR	$2.30 \pm .10$	$0.410 \pm .006$	$2.08 \pm .07$	$0.373 \pm .005$
	J	$2.60 \pm .13$	$0.398 \pm .007$	$2.28 \pm .09$	$0.385 \pm .005$
	L	$3.17 \pm .14$	$0.376 \pm .008$	$2.62 \pm .09$	$0.400 \pm .004$
097	VISAR	$2.79 \pm .15$	$0.62 \pm .01$	$3.87 \pm .16$	$0.347 \pm .007$
	I	$3.16 \pm .05$	$0.60 \pm .01$	$4.22 \pm .09$	$0.361 \pm .003$
	J	$3.14 \pm .10$	$0.60 \pm .01$	$4.20 \pm .12$	$0.361 \pm .004$
	K	$3.18 \pm .10$	$0.59 \pm .01$	$4.24 \pm .12$	$0.362 \pm .004$
	L	$3.04 \pm .09$	$0.60 \pm .01$	$4.11 \pm .11$	$0.357 \pm .004$
094	VISAR	$3.12 \pm .07$	$0.84 \pm .02$	$5.86 \pm .15$	$0.326 \pm .005$
	J	$3.41 \pm .08$	$0.82 \pm .02$	$6.25 \pm .17$	$0.340 \pm .004$
	L	$3.64 \pm .05$	$0.80 \pm .02$	$6.53 \pm .16$	$0.348 \pm .003$

Table 7. Dry ATC DSTS Impedance Match Data

Shot	Measurement	U_s	u_p	P	ν
119	VISAR	$0.88 \pm .11$	$0.274 \pm .003$	$0.42 \pm .05$	$0.39 \pm .02$
	I	$0.89 \pm .03$	$0.273 \pm .001$	$0.43 \pm .01$	$0.40 \pm .07$
	J	$0.98 \pm .01$	$0.271 \pm .001$	$0.465 \pm .006$	$0.414 \pm .003$
	K	$0.95 \pm .02$	$0.273 \pm .001$	$0.43 \pm .01$	$0.397 \pm .005$
	L	$0.89 \pm .03$	$0.274 \pm .001$	$0.42 \pm .01$	$0.396 \pm .006$
114	VISAR	$1.32 \pm .04$	$0.434 \pm .003$	$1.06 \pm .03$	$0.375 \pm .007$
	I	$1.32 \pm .02$	$0.464 \pm .003$	$1.05 \pm .01$	$0.374 \pm .003$
	J	$1.33 \pm .03$	$0.463 \pm .003$	$1.07 \pm .02$	$0.377 \pm .006$
	K	$1.32 \pm .03$	$0.464 \pm .003$	$1.06 \pm .02$	$0.375 \pm .005$
	L	$1.39 \pm .01$	$0.461 \pm .003$	$1.11 \pm .01$	$0.386 \pm .003$
121	VISAR	$1.90 \pm .03$	$0.665 \pm .006$	$2.19 \pm .04$	$0.376 \pm .005$
	I	$1.80 \pm .03$	$0.671 \pm .006$	$2.09 \pm .04$	$0.363 \pm .005$
	J	$1.89 \pm .02$	$0.666 \pm .006$	$2.18 \pm .03$	$0.375 \pm .003$
	K	$1.87 \pm .02$	$0.667 \pm .006$	$2.15 \pm .03$	$0.371 \pm .003$
	L	$1.82 \pm .04$	$0.670 \pm .006$	$2.11 \pm .05$	$0.365 \pm .006$
124	VISAR	$2.47 \pm .03$	$0.94 \pm .01$	$4.16 \pm .07$	$0.346 \pm .005$
	I	$2.58 \pm .01$	$0.93 \pm .01$	$4.30 \pm .06$	$0.356 \pm .003$
	J	$2.44 \pm .02$	$0.94 \pm .01$	$4.12 \pm .06$	$0.343 \pm .003$
	K	$2.38 \pm .02$	$0.95 \pm .01$	$4.03 \pm .06$	$0.335 \pm .004$
	L	$2.53 \pm .01$	$0.93 \pm .01$	$4.24 \pm .06$	$0.352 \pm .003$

Table 8.   Wet ATC DSTS Impedance Match Data

Shot	Measurement	U_s	u_p	P	ν
128	VISAR	$2.97 \pm .21$	$0.223 \pm .005$	$1.51 \pm .08$	$0.406 \pm .004$
	I	$2.92 \pm .06$	$0.224 \pm .003$	$1.49 \pm .03$	$0.405 \pm .002$
	J	$2.92 \pm .08$	$0.224 \pm .003$	$1.49 \pm .03$	$0.405 \pm .002$
	K	$2.94 \pm .08$	$0.224 \pm .003$	$1.50 \pm .03$	$0.406 \pm .002$
	L	$2.97 \pm .06$	$0.223 \pm .003$	$1.51 \pm .03$	$0.406 \pm .002$
127	VISAR	$3.16 \pm .21$	$0.343 \pm .009$	$2.44 \pm .12$	$0.396 \pm .005$
	I	$3.12 \pm .08$	$0.345 \pm .006$	$2.42 \pm .06$	$0.395 \pm .003$
	J	$3.18 \pm .07$	$0.343 \pm .006$	$2.45 \pm .06$	$0.396 \pm .002$
	K	$3.14 \pm .05$	$0.344 \pm .005$	$2.43 \pm .05$	$0.396 \pm .002$
	L	$3.03 \pm .04$	$0.347 \pm .005$	$2.37 \pm .04$	$0.393 \pm .002$
130	VISAR	$3.43 \pm .13$	$0.536 \pm .012$	$4.20 \pm .14$	$0.367 \pm .004$
	I	$3.62 \pm .04$	$0.53 \pm .01$	$4.37 \pm .09$	$0.372 \pm .002$
	J	$3.68 \pm .04$	$0.52 \pm .01$	$4.42 \pm .10$	$0.373 \pm .002$
	K	$3.66 \pm .04$	$0.52 \pm .01$	$4.40 \pm .09$	$0.373 \pm .002$
	L	$3.58 \pm .05$	$0.53 \pm .01$	$4.34 \pm .09$	$0.371 \pm .001$
129	VISAR	$3.90 \pm .16$	$0.77 \pm .02$	$6.93 \pm .25$	$0.348 \pm .005$
	I	$4.14 \pm .07$	$0.75 \pm .02$	$7.21 \pm .20$	$0.354 \pm .003$
	J	$4.21 \pm .08$	$0.75 \pm .02$	$7.29 \pm .21$	$0.356 \pm .003$
	K	$4.19 \pm .08$	$0.75 \pm .02$	$7.27 \pm .20$	$0.355 \pm .003$
	L	$4.06 \pm .05$	$0.76 \pm .02$	$7.12 \pm .18$	$0.352 \pm .002$